$$H_{9\text{B3}} = \frac{1.808 \cdot 10^{14}}{s^3 + 1.131 \cdot 10^5 s^2 + 6.396 \cdot 10^9 s + 1.808 \cdot 10^{14}} , \quad (5)$$

$$H_{9\text{C3}} = \frac{4.531 \cdot 10^{13}}{s^3 + 3.377 \cdot 10^4 s^2 + 2.969 \cdot 10^9 s + 4.531 \cdot 10^{13}} . \quad (6)$$

For the impedance-based techniques, since $f_s = 960$ Hz (see section II-B), the anti-aliasing f_c must be, at most, 480 Hz. Here, $f_c = 180$ Hz was used. The second order Butterworth transfer function ($H_{180\text{B2}}$), the third order Butterworth transfer function ($H_{180\text{B3}}$), and the third order Chebyshev transfer function ($H_{180\text{C3}}$) are described in (7), (8), and (9), respectively.

$$H_{180\text{B2}} = \frac{1.279 \cdot 10^6}{s^2 + 1599 s + 1.279 \cdot 10^6} , \quad (7)$$

$$H_{180\text{B3}} = \frac{1.447 \cdot 10^9}{s^3 + 2262 s^2 + 2.558 \cdot 10^6 s + 1.447 \cdot 10^9} , \quad (8)$$

$$H_{180\text{C3}} = \frac{3.625 \cdot 10^8}{s^3 + 675.5 s^2 + 1.187 \cdot 10^6 s + 3.625 \cdot 10^8} . \quad (9)$$

The ideal and anti-aliasing filters frequency responses for $f_c = 180$ Hz and $f_c = 9$ kHz are shown in Fig. 1.

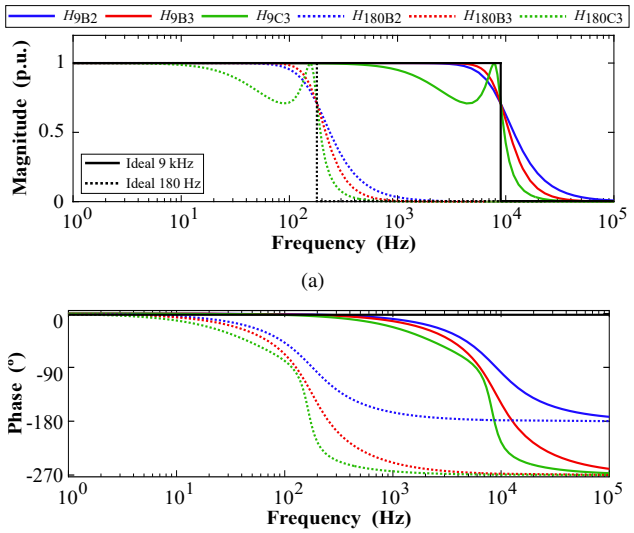

Fig. 1. Ideal, Butterworth, and Chebyshev frequency responses: (a) magnitude; (b) phase.

B. Analyzed IT

During faults on TL, the IT secondary signals may present transient components not found at the primary waveforms, which may lead to fault locators and relays misoperations [1]. In this paper, the transient behavior of two 230 kV CCVTs and one CT models are evaluated. The CCVTs are named as CCVT 1 and CCVT 2, and the required circuit topology and parameters are reported in [13], p. 42, and [14], p. 2 and 8, respectively. The CT parameters are described in [13], p. 41.

The CCVT 1, CCVT 2, and CT frequency responses are shown in Figs. 2, 3, and 4, respectively, which were obtained using the ATP Frequency Scan routine [7]. The frequency response of the conjunction of IT and anti-aliasing filters are also shown in the same figures. The frequency responses are plotted considering primary signals (K_{pri}), secondary signals (K_{s}), secondary and second order Butterworth filters with $f_c = 9$ kHz ($K_{\text{s B2}}$) and $f_c = 180$ Hz ($K_{\text{s 180B2}}$), secondary and third order Butterworth filters with $f_c = 9$ kHz ($K_{\text{s B3}}$) and $f_c = 180$ Hz ($K_{\text{s 180B3}}$), and secondary and third order Chebyshev filters with $f_c = 9$ kHz ($K_{\text{s C3}}$) and $f_c = 180$ Hz ($K_{\text{s 180C3}}$), where K is V for voltage or I for current waveforms. The primary and secondary signals were normalized in per unit values in order to make possible some comparative analysis. The angle responses are presented in degrees. Despite the CCVT 2 shows an unusual magnitude frequency response (see Fig. 3(a)), all of its parameters were obtained from laboratory measurements [14].

At fundamental frequency, the IT present acceptable accuracy once the secondary voltages and currents are quite similar to the respective primary waveforms (see Figs. 2, 3, and 4), even when the anti-filters are taken into account. However, when the power network goes through a transient state, the secondary voltages differs from the primary signals in such a way that off-nominal frequency components are amplified or attenuated depending on the CCVTs frequency responses, which can affect high frequency measurements accuracy and protective relaying algorithms' performances. Regarding to the CT transient behavior, a typical CT model presents a magnitude frequency response constant over a wide frequency range (up to 50 kHz). For practical purposes, the CT may be regarded as having no impact on the spectral content of the input current signal, under conditions of the ferromagnetic core is not saturated [2]. On the other hand, when the anti-aliasing filters are considered, the secondary currents may be distorted in relation to the respective primary current (see Fig. 4).

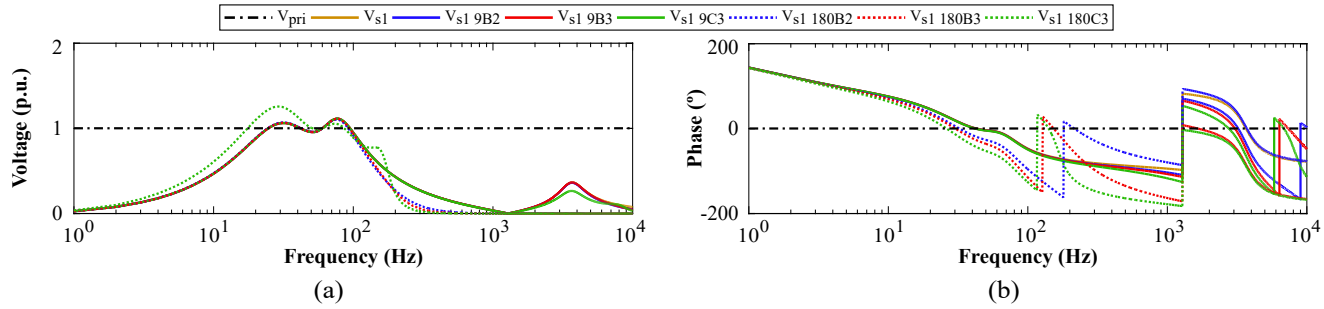

Fig. 2. CCVT 1 frequency response: (a) magnitude (p.u.); (b) phase (°).

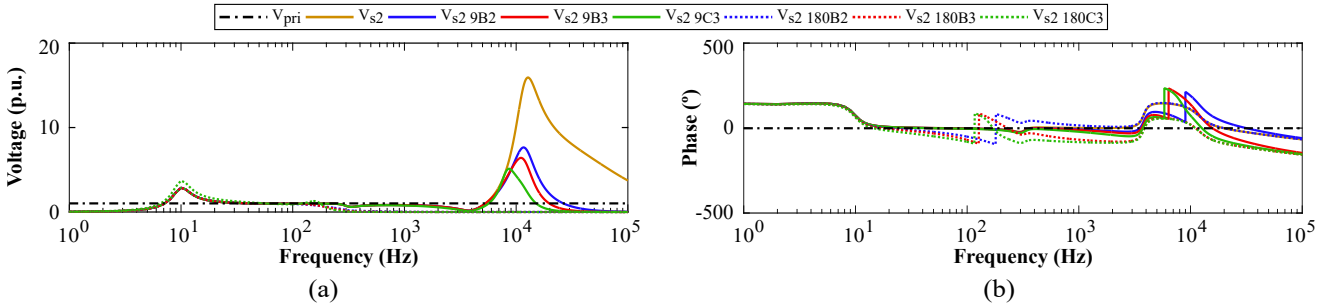

Fig. 3. CCVT 2 frequency response: (a) magnitude (p.u.); (b) phase (°).

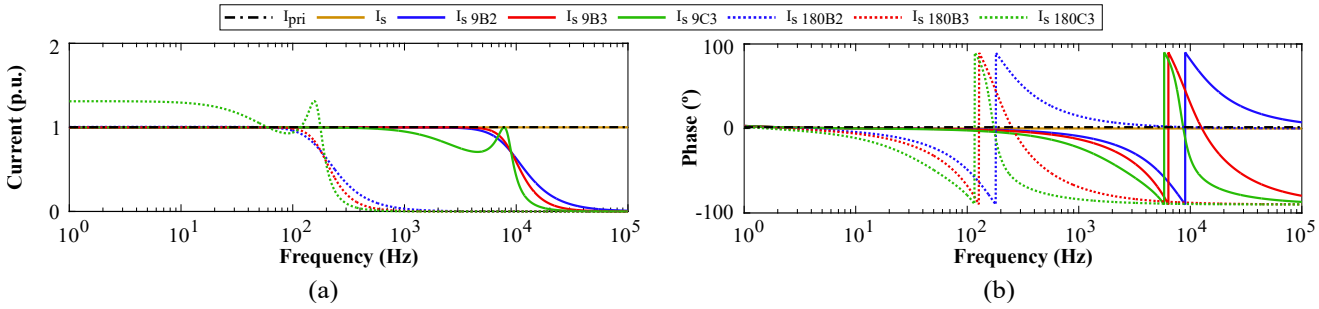

Fig. 4. CT frequency response: (a) magnitude (p.u.); (b) phase (°).

The dynamic behavior of each analyzed IT in time domain is shown in Fig. 5 for a single line to ground fault located at 25 km away from the monitored bus on a 230 kV electric power system, which is described in section IV.

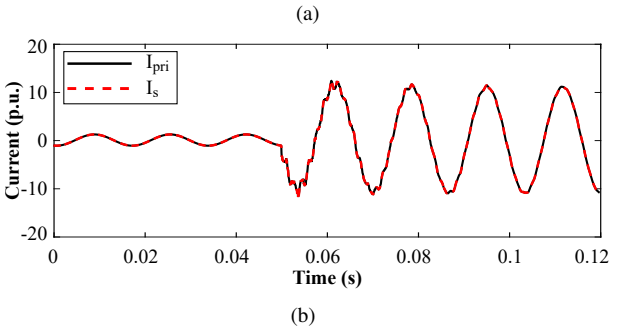

Fig. 5. Secondary waveforms due to a single line to ground fault: (a) voltage; (b) current.

From Fig. 5(a), it is noticeable that CCVT 1 and CCVT 2 secondary voltages (V_{s1} and V_{s2}, respectively) do not adequate follow the primary voltage waveform (V_{pri}) after the fault inception. V_{s2} significantly amplifies the high frequency components, according to its frequency response (see Fig. 3(a)). On the other hand, V_{s1} presents considerable attenuations on the off-nominal frequencies (see Fig. 2(a)). In both V_{s1} and V_{s2}, some phase displacements in relation to V_{pri} are presented as well. In the case of current measurements depicted in Fig. 5(b), since the electromagnetic flux in the CT core is operating in the linear region, the secondary current signal (I_s) is almost an ideal replica of the primary current (I_{pri}). In this way, the IT transient behavior may affect the secondary measurements and transfer undesired information to fault locators.

IV. Analysis and Results

Several ATP fault simulations were performed in the power network shown in Fig. 6, which is based on the one proposed in [13] for protection studies, in order to evaluate the impact of the analyzed IT and anti-filters on the fault locators. All the short-circuits were applied in TL 3. The line length of each TL is 150 km. The ATP time step was chosen as 2 μs.

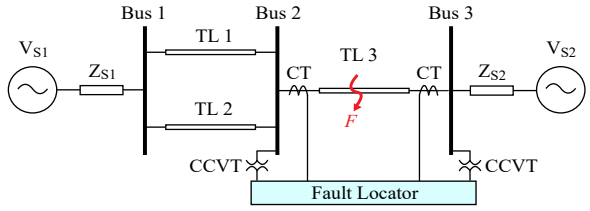

Fig. 6. 230 kV electric power system used in ATP simulations.

After each simulation, the fault point is estimated considering as input signals to the fault location algorithms the primary signals, secondary waveforms, and filtered secondary signals. Here, the primary signals are taken as reference. In the cases of travelling wave-based evaluations, the fault distance is estimated considering only voltage samples as input data, only current samples as input, and both voltage and current samples simultaneously. In situations that voltage and current samples are available concomitantly, the first fault-induced transient is detected in relation to the first incident wave reaching the monitored TL bus, whether it is voltage or current.

A total amount of 1050 fault scenarios were performed for each analyzed signal[1]. In each simulation, the fault inception angle, fault resistance, fault type, and fault location were varied. The simulation variables are shown in Table I.

TABLE I
SIMULATION VARIABLES USED IN EACH FAULT SITUATION

Simulation variables	Values
Fault location (km)	25, 50, 75, 100, 125
Fault type	AG, BG, CG, AB, BC, CA, ABG, BCG, CAG, ABC
Inception angle (°)	0, 30, 60, 90, 120, 150, 180
Fault resistance (Ω)	0.1, 1, 7

The fault location relative error ϵ_k is computed as:

$$\epsilon_k(\%) = \frac{|d - \tilde{d}_k|}{\ell} \cdot 100 \ , \tag{10}$$

where d is the actual fault location, $\tilde{d}_k$ is the estimated fault distance, ℓ is the TL length, and k is the input signal (primary, secondary, or filtered secondary samples). Considering that f_s is 50 kHz and v was taken in this paper as 98% of the speed of light in free space, the maximum admissible error is 5.88 km ($\Delta t \cdot v$), which is approximately 3.9% of the TL length. Since ϵ_k is computed after each simulation, an error function is generated from the total amount of fault cases, whose obtained average values μ_ϵ and standard deviations σ_ϵ are shown in Table II for the travelling wave-based techniques.

TABLE II
INFLUENCE OF IT ON TRAVELLING WAVE-BASED FAULT LOCATORS

Relative errors (%)	Monitored signals*	Analyzed IT				
		CCVT 1	CCVT 2	CT	CCVT 1 & CT	CCVT 2 & CT
μ_ϵ	K_{pri}	0.498	0.498	0.495	0.498	0.498
	K_{s}	0.519	0.485	0.492	0.492	0.498
	$K_{\text{s 9B2}}$	0.649	0.476	0.501	0.502	0.471
	$K_{\text{s 9B3}}$	0.536	0.532	0.548	0.532	0.492
	$K_{\text{s 9C3}}$	0.677	0.570	0.684	0.677	0.575
σ_ϵ	K_{pri}	0.567	0.566	0.564	0.566	0.566
	K_{s}	0.571	0.557	0.562	0.561	0.566
	$K_{\text{s 9B2}}$	0.586	0.545	0.552	0.551	0.540
	$K_{\text{s 9B3}}$	0.594	0.593	0.603	0.592	0.560
	$K_{\text{s 9C3}}$	0.679	0.599	0.683	0.678	0.601

* K is the V or I samples, depending on the analyzed IT. In cases which both V and I samples are simultaneously available, as in CCVT 1 & CT and CCVT 2 & CT, K means V and I.

To investigate in more detail the travelling wave-based fault locator's performance, the percentage errors are presented as boxplots in Fig. 7, which are plots able to visually reveal some basic statistics of a data set, using five thresholds: the maximum value, represented by the upper whisker; the upper quartile, represented by the upper boundary of the box; the median quartile, represented by the intermediate line inside the box; the lower quartile, represented by the lower boundary of the box; and the minimum value, represented by the lower whisker. The upper quartile, the median and the lower quartile represent the maximum fault location error in 75%, 50% and 25% of the simulated fault cases, respectively.

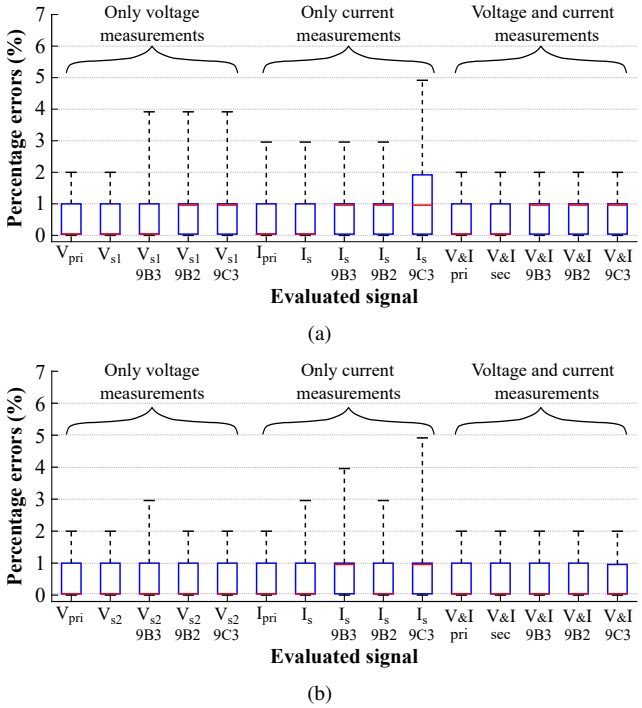

Fig. 7. Boxplots representing the travelling wave-based fault location percentage erros: (a) CCVT 1 and CT; (b) CCVT 2 and CT.

From the results presented in Table II and in Fig. 7, when only voltage measurements are available at the monitored buses, the μ_ϵ and σ_ϵ results are higher for the CCVT 1 secondary and filtered secondary samples than the ones obtained with the reference signal (V_{pri}). In fact, CCVT 1 frequency response significantly attenuates high frequencies (see Fig. 2(a)), which affects the fault-induced transient detection processes since they are more sensitive to the highest frequency spectrum. On the other hand, the μ_ϵ and σ_ϵ are smaller than the ones computed by V_{pri} when the CCVT 2 secondary and filtered secondary waveforms are taken as input data. In these scenarios, the travelling wave-based fault locator's performance was improved once CCVT 2 transient behavior amplifies high frequencies (see Fig. 3(a)), which makes the fault-induced transient detection procedure easier. When only current measurements are available, the fault distances are estimated more accurate than when the CCVT 1 secondary voltages were considered as input data. However, the best results were obtained when voltage and current signals are available simultaneously. In these cases, the maximum errors were smaller than when only voltage or current measurements were available, irrespective to the analyzed CCVT (see Fig. 7), indicating that the travelling wave-based fault locator's performance is more accurate and reliable. Regarding the solutions computed with the filtered secondary signals, the second order Butterworth filter has shown to be more appropriate to be used in cascade with the IT analog signals. The third order Chebyshev filter has shown the poorest results, which may be

[1] 1050 fault simulations when V_{pri} is taken as input data for the travelling wave-based fault locator, 1050 fault simulations when V_{pri} and I_{pri} are taken as input data for the impedance-based techniques, etc.

due to the oscillations presented in the bandpass (see Fig. 1(a)). In addition to it, the maximum admissible error was only exceeded with the use of this filter in cascade with secondary current signals (see Fig. 7). It should be pointed out that smaller errors would be achieved for higher sampling rates. However, irrespective to the sampling rate used, the CCVT secondary voltage may be quite different from the primary voltage during faults (see Fig. 5(a)). In such cases, information not found at the primary side can be transferred to the fault locators as input data, affecting the fault locators' performance.

The obtained μ_ϵ and σ_ϵ for the impedance-based algorithms are shown in Table III.

TABLE III
INFLUENCE OF IT ON IMPEDANCE-BASED FAULT LOCATORS

Analyzed IT	Monitored signals*	One-ended Method		Two-ended Method	
		μ_ϵ	σ_ϵ	μ_ϵ	σ_ϵ
CCVT 1 & CT	K_{pri}	1.072	1.316	0.250	0.221
	K_{s}	1.084	1.413	0.414	0.386
	$K_{\text{s 180B2}}$	0.782	1.394	0.421	0.383
	$K_{\text{s 180B3}}$	0.782	1.393	0.421	0.383
	$K_{\text{s 180C3}}$	0.831	1.395	0.455	0.412
CCVT 2 & CT	K_{pri}	1.076	1.325	0.219	0.185
	K_{s}	1.085	1.326	0.585	0.680
	$K_{\text{s 180B2}}$	0.503	1.054	0.146	0.100
	$K_{\text{s 180B3}}$	0.493	1.053	0.146	0.100
	$K_{\text{s 180C3}}$	0.525	1.067	0.165	0.125

* K means V and I samples, depending on the analyzed IT.

From the results shown in Table III, the best solutions were obtained by the two-ended method, as was expected since two-terminal techniques use more input data to estimate the fault point. The μ_ϵ and σ_ϵ for both one- and two-terminal algorithms were higher than the ones obtained with the reference signals when the secondary waveforms were considered. Particularly to the CCVT 2 and CT results, the μ_ϵ and σ_ϵ were higher than the ones obtained with CCVT 1 and CT. In fact, the high frequency components amplified by the CCVT 2 transient behavior (see Fig. 3(a)) affect the phasor estimation procedure, which in turn compromise the fault location performance. Considering the filtered secondary samples as input data, the second and third order Butterworth filters have shown to be more suitable to be used in conjunction with the IT outputs, with the third order Butterworth filter showing slightly better results. In general, the results obtained with the usage of anti-aliasing filters were better since frequency components higher than f_c are attenuated, which improves the phasor estimation performance and, consequently, the fault location procedure. The worst solutions were provided by the Chebyshev filter, probably due to the oscillations at the bandpass (see Fig. 1(a)).

V. CONCLUSION

The impact of two CCVT and one CT in cascade with three different analog low-pass anti-aliasing filters on a two-ended travelling wave-based and one- and two-terminal impedance-based fault techniques were investigated. Several ATP fault simulations were performed varying fault parameters as resistance, inception angle, location, and type. In each simulation, the fault point was estimated using the primary, secondary, and filtered secondary signals as input to the fault locators.

From the obtained results, the travelling wave-based performance was more affected when CCVT transient behavior attenuates high frequency components, since this technique is more sensitive to higher frequencies. In cases in which the CCVT amplifies high frequencies, the performance was improved. However, the best solutions were found when both voltage and current samples were available simultaneously. Regarding the anti-aliasing filters, the second order Butterworth filter has shown to be more appropriate for travelling wave-based applications.

In relation to the impedance-based routines, the two-ended method has shown to be more immune to the IT transient behavior. However, the poorest results were found when the CCVT amplifies high frequencies, which may affect the phasor estimation procedure, and, consequently, the fault locator's performance. The use of anti-aliasing filters provided better results once frequency components higher than the cut-off frequency are attenuated, which improves the phasor estimation the fault location performances. In both travelling wave-based and impedance-based analysis, the highest errors were computed when the Chebyshev filter were used.

REFERENCES

[1] M. M. Saha, J. Izykowski, and E. Rosolowski, *Fault Location on Power Networks*, ser. Power Systems. London: Ed. Springer, 2010.

[2] B. Naodovic, "Influence of instrument transformers on power system protection," Ph.D. dissertation, Texas A&M University, 2005.

[3] A. G. Phadke and J. S. Thorp, *Computer Relaying for Power Systems*, 2nd ed., ser. Protective relays. England: A John Wiley and Sons Ltd, 2009.

[4] R. L. A. Reis, F. V. Lopes, W. L. A. Neves, and D. F. Jr., "Influence of coupling capacitor voltage transformers on travelling wave-based fault locators," *International Conference on Power Systems Transients*, June 2015.

[5] D. Hou and J. Roberts, "Capacitive voltage transformer: transient overreach concerns and solutions for distance relaying," in *Electrical and Computer Engineering, 1996. Canadian Conference on*, vol. 1, May 1996, pp. 119–125 vol.1.

[6] F. B. Costa, "Fault-induced transient detection based on real-time analysis of the wavelet coefficient energy," *IEEE Transactions on Power Delivery*, vol. 29, no. 1, pp. 140–153, Feb 2014.

[7] *ATP - Alternative Transient Program*, Leuven EMTP Center, Herverlee, Belgium, 1987.

[8] P. F. Gale, P. A. Crossley, X. Bingyin, G. Yaozhong, B. J. Cory, and J. R. G. Barker, "Fault location based on travelling waves," in *Developments in Power System Protection, 1993., Fifth International Conference on*, 1993, pp. 54–59.

[9] S. L. Zimath, M. A. F. Ramos, and J. E. S. Filho, "Comparison of impedance and travelling wave fault location using real faults," in *IEEE PES T D 2010*, April 2010, pp. 1–5.

[10] S. Das, S. Santoso, A. Gaikwad, and M. Patel, "Impedance-based fault location in transmission networks: theory and application," *IEEE Access*, vol. 2, pp. 537–557, 2014.

[11] T. Takagi, Y. Yamakoshi, M. Yamaura, R. Kondow, and T. Matsushima, "Development of a new type fault locator using the one-terminal voltage and current data," *IEEE Transactions on Power Apparatus and Systems*, vol. PAS-101, no. 8, pp. 2892 –2898, aug. 1982.

[12] G. Benmouyal, "Removal of dc-offset in current waveforms using digital mimic filtering," *IEEE Transactions on Power Delivery*, vol. 10, no. 2, pp. 621–630, Apr 1995.

[13] *EMTP Reference Models for Transmission Line Relay Testing*, IEEE Power System Relaying Committee, 2004. [Online]. Available: http://www.pes-psrc.org

[14] A. V. Carvalho, A. R. F. Freire, and H. M. de Oliveira, "Transient interaction between coupling capacitors voltage transformers and transmission lines," in *2009 IEEE Power Energy Society General Meeting*, July 2009, pp. 1–8.